Experimental Demonstration of the Production of Hydrogen and Water-Free Formaldehyde Using Sodium Vapor

Marta Kamienowska, Max Philipp Deutschmann, Michael Bender, Leonid Stoppel, Markus Daubner, Thomas Wetzel and Klarissa Niedermeier*

Supporting Information available online

Conventional routes for the production of formaldehyde rely on the use of methanol and air, with the presence of catalysts such as silver or mixed-metal oxides. These processes are highly energy intensive and therefore raise concerns in terms of cost-effectiveness and environmental impact. In that respect, sodium or sodium compounds are more favorable as catalysts for the direct dehydrogenation of methanol to water-free formaldehyde. A method is presented for the coproduction of hydrogen and anhydrous formaldehyde – both valuable products – on the laboratory scale, with a particular focus on the design and testing of a sodium vapor catalyst dosing unit that enables the process to be performed continuously.

1 Introduction

Formaldehyde is an important organic compound with a vital role in a wide range of industrial sectors. It is used as a precursor in the synthesis of many products, such as resins, plastics, fertilizers, and textiles [1–3]. Its wide range of applications makes formaldehyde an essential part of today's chemical industry. Several methods have been developed on the industrial scale for the production of formaldehyde, such as the water ballast process (BASF Process), the methanol ballast process, and the Formox process. All of these approaches generally require energy-intensive steps for the workup of the crude liquid product. For the water ballast process, this implies the removal of water, and in the methanol ballast process, separation of methanol [4]. In the case of the Formox route, the short life of the iron molybdate catalyst is indeed a major concern, affecting both the economic and the operational efficiency of the production [5]. Moreover, a common difficulty is also the achievement of highly concentrated formaldehyde. Knowing the drawbacks of the mentioned industrial processes, researchers have been trying to develop a more efficient way to produce formaldehyde for more than three decades now. Furthermore, the development of the target reaction converting methanol (MeOH) to formaldehyde (HCHO) and hydrogen

(H_2) offers significant advantages. Anhydrous formaldehyde can be processed into various chemical products without the interference of water as the main by-product from conventional, oxidative processes. In addition, hydrogen is co-generated in this reaction as a very valuable by-product that can be used in a multitude of hydrogenation processes – towards many different chemicals or fuels.

Compounds of transition metals such as zinc, silver, and copper have been identified as promising catalysts [6]. These metals, either in their elemental state or in various modified forms, have shown some degree of activity in the dehydrogenation reaction. Yet, sodium compounds have

———————

[1,2]M.Sc. Marta Kamienowska, [2]M.Sc. Max Philipp Deutschmann,
[1]Dr. Michael Bender, [2]Dr.-Ing. Leonid Stoppel,
[2]Dipl.-Ing. Markus Daubner, [2]Prof. Dr.-Ing. Thomas Wetzel,
[2]Dr.-Ing. Klarissa Niedermeier
https://orcid.org/0000-0003-0828-7299
(klarissa.niedermeier@kit.edu)
[1]BASF SE, Carl-Bosch-Strasse 38, 67056 Ludwigshafen am Rhein, Germany.
[2]Karlsruhe Institute of Technology, Institute for Thermal Energy Technology and Safety (ITES), Hermann-von-Helmholtz-Platz 1, 76344 Eggenstein-Leopoldshafen, Germany.

been identified as the most promising ones. According to the theory derived from the work of Sauer and Emig [7], sodium aluminate would release a catalytically active component into the gas phase, which has been found to catalyze methanol dehydrogenation homogenously (Eq. (1)).

$$CH_3OH \rightleftarrows H_2 + HCHO \ \Delta H = 84 \frac{kJ}{mol} \qquad (1)$$
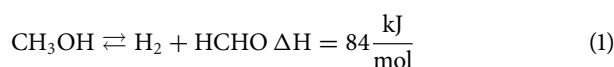
To confirm this statement, Ruf and Emig [8] and Maurer and Renken [9] conducted a series of experiments using elemental sodium as a catalyst in the methanol dehydrogenation process. Ruf [10] proposed several approaches to the sodium dosing method for this reaction. One of them involved placing metallic sodium in a ceramic boat and heating it in a methanol stream. The experiments showed that sodium homogeneously catalyzed the dehydrogenation of methanol. When the ceramic boat was removed, it was found that most of the sodium had been consumed, leaving mainly residues of sodium oxide or sodium hydroxide. Ruf and Emig [8] estimated the amount of evaporated sodium by weighing the ceramic boat before and after the reaction. The use of a ceramic boat raised practical issues in achieving a continuous and controlled flow of evaporated sodium. These challenges were recognized as hindering the experimental accuracy and reproducibility. To overcome this issue, Ruf et al. introduced a bubble column concept, which is described in detail in [11]. In general, the bubble column concept involves feeding sodium vapor and inert gas into a reaction system. This technique provided a dosage of small amounts of sodium, ensuring feed of catalyst to the reaction.

An important issue when using sodium in a stainless-steel reactor system is corrosion. Therefore, there has been extensive research into the problem of corrosion in stainless-steel systems, particularly when sodium is used as a coolant in fast reactors [12–14]. A number of methods are considered to mitigate the corrosive effects of sodium on stainless-steel systems. Research is underway to develop advanced steel alloys that are more resistant to corrosion caused by sodium [15–17]. There is also interest in coating materials to inhibit corrosion induced by liquid metals [18–21]. In addition, purification systems are used to reduce impurities that contribute to metal decay [22]. In this study, the choice of the materials and the purification technique was made based on previous research, in particular, the use of zirconium foil as a sodium purifier agent [22]. Within this work, the sodium evaporation and condensation experiments were conducted in order to quantify the amount of sodium evaporated, using the concept of a bubble column as the basis of the experimental design. This approach allowed a controlled and constant dosage of sodium, thereby enabling the continuous production of formaldehyde and hydrogen on the mini-plant scale, which has not been done, so far.
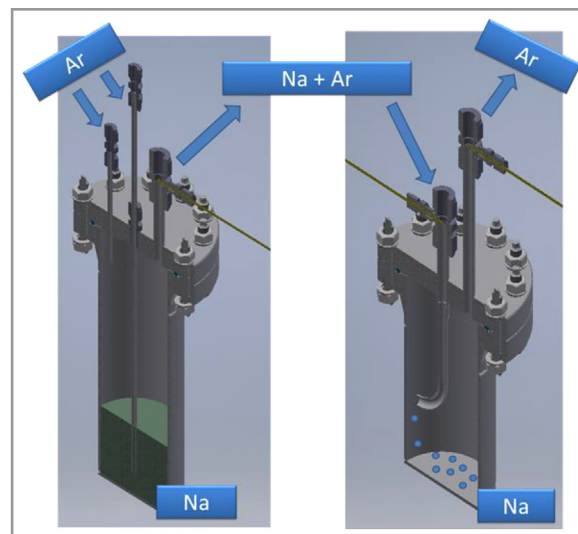
Figure 1. Technical ilustration of the sodium evaporator (left) and the condenser (right).

2 Materials and Experimental Setup

2.1 Sodium Evaporation and Condensation

In order to determine the optimum parameters of the catalyst dosing system for the methanol dehydrogenation tests, a setup for sodium evaporation and condensation was designed and built. Fig. 1 shows a technical ilustration of the sodium evaporation and condensation system. The process flow diagram is presented in Fig. 2.

The system operates by means of a 1.3-L bubble column in which sodium is heated by a 700-W heating jacket. Two independent flow regulators (F-201CV-2K0-PGD-33-K; Bronkhorst) control the argon flow: one for a shortened pipe (FC.1) and the other for the primary bubble pipe (FC.2). After the evaporation phase, the sodium is condensed in a dedicated container kept at about −20 °C, which is placed in a cooling bath filled with silicone oil. At the end of each experiment, the condenser was inspected, and the sodium was usually found at the bottom of the condenser or adhering to the inner wall, or a combination of the two (Fig. 3). The gathered amount of evaporated sodium was weighed.

The temperatures inside the pipes and at the entrance and exit of the containers were measured with thermocouples (Type K, class 1 in accordance with IEC 60584, Inconel 600, insulation MgO, outer diameter (OD) 3 mm). The pipelines were heated up using heating tapes (Horst). The pressure in the system was measured using a Rosemount 2051 in-line pressure transmitter from Emerson. There is also a backpressure controller (P-502C-1K1R-PGD-39-K + F-001AV-LFU-33-K) provided by Bronkhorst, which allows the pressure to be controlled in the experimental setup.
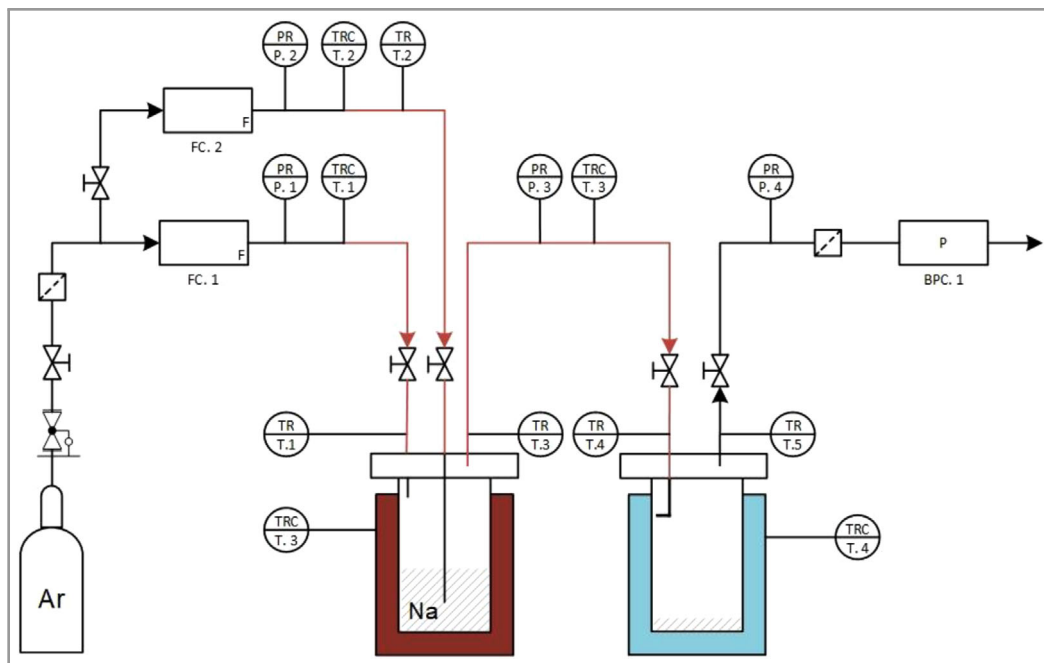
Figure 2. Process flow diagram of the entire sodium evaporation and condensation setup.

The sodium bubble column operated in this work was based on the concept of Ruf et al. [11]. However, a number of modifications were made to the setup of Ruf et al. to improve the process stability and to meet specific operational requirements (Tab. 1). In order to provide the increased capacity of the mini-plant, a scale-up of the setup was performed.

A secondary flow controller was integrated to provide full management of the gas flow through the bubble pipe, i.e., allowing for a consistent flow regime, limiting potential thermal disturbances, and thus consolidating the operational stability of the system. To complement this, a backpressure controller was added to provide pressure

modulation capabilities, ensuring that the operating parameters were consistently maintained within the specified optimum and safety thresholds. Sodium of two purities was tested, i.e., 99.8 % manufactured by Sigma-Aldrich and ExcelAR reagent (ER)-grade 99.98 % from Métaux Spéciaux. The chemical compositions of the tested sodium are presented in Tab. 2.

Table 1. Comparison between the previously tested column and own work.

Sodium bubble column	This work	Ruf [10]
Volume [L]	1.3	0.1
Height [mm]	248	120
Inner diameter [mm]	82.5	34
Inert gas dosing	2 flow controllers	1 flow controller
Purification system	Zr foil	none
Sodium loading	up to 800 g	up to 60 g

Figure 3. Picture of evaporated sodium in the condenser after an experiment.

Table 2. Chemical composition of the tested sodium.

	Trial 1	Trial 2
	S+ grade	ER grade
Na [%]	99.80	99.98
Ca [ppm]	<400	<10
K [ppm]	<300	<10
Cl + Br [ppm]	<20	<20

Figure 4. MEDENA setup.

2.2 Methanol Dehydrogenation Mini-Plant (MEDENA)

The experimental tests of methanol dehydrogenation were conducted in a self-constructed laboratory setup (Fig. 4).

A process flow diagram of the given system is presented in Fig. 5. First, methanol and argon (stream 1) as well as the sodium and argon (stream 2) were preheated and fed into the reactor. The dehydrogenation reaction took place in a tubular reactor (inner diameter (ID) = 10 cm, $L = 45$ cm) made of Alloy 625 (2.4856) at $T = 500$–900 °C and $p = 1.2$ bar. The reactor was heated by means of a 3000-W electric oven with three heating zones. The methanol concentration was varied between 2.5 and 20 wt % for the set of experiments presented. The methanol flow rate was set at 10 and 20 g h^{-1} with the appropriate amount of argon flow. Different amounts of catalyst were tested, with values ranging from 0.05 to 0.3 g h^{-1}. The temperatures inside the pipes and reactor were measured with thermocouples (as in Sect. 2.1). The pressure in the system was measured using the same equipment as mentioned in Sect. 2.1. There is also a backpressure controller (identical to the one used in Sect. 2.1) that allows partial control over the pressure in the plant.

The product stream was analyzed using a gas chromatograph (GC; ARNEL 6453, Perkin Elmer) equipped with a main column (Molesieve 5A), which is protected by a precolumn (Plot U) that efficiently removes contaminants from the gas stream by a backflush-to-vent system using a two-valve-switch in an external, heated GC equipped with a thermal conductivity detector, a methanizer, and a flame ionization detector. Argon (99.9999 %; Air Liquide), used as the carrier gas, was passed through an oxygen, a moisture, and a hydrocarbon trap (Restek) for additional purification. A flow controller (F-201CV-050-PGD-33-K) provided by Bronkhorst was installed in order to provide a constant flow through the GC valves.

The experimental uncertainty of the results obtained during trials is estimated to be 15 % (up to 20 % for higher flows of >2 L min^{-1}) due to the varying pressure in the system. Methanol (99.9 %, extra dry; AcroSeal) was supplied using a mass flow controller (FC.4; ML120V00-PGD-33-0-S-DA-000; Bronkhorst) and an evaporator (W-202A-330-K; Bronkhorst), in which methanol and argon were heated to 120 °C. Stainless-steel (316) pipes for the methanol stream were coated with Silcolloy 1000, which is a hydrogenated amorphous silicon coating manufactured by SilcoTek® GmbH. Argon (99.9999 %; Air Liquide) was dosed by a F-201CV-2K0-PGD-33-K (Bronkhorst) and it was used as a dilutant gas. Moreover, it was passed through a 0.5-micron pore size particulate filter provided by Swagelok. The non-analyzed product stream was absorbed in water solution in a gas scrubber.

Due to the corrosive nature of sodium and the experience gained from the previous sodium experiments, the reactor and other key parts of the system were coated with a protective layer of aluminum oxide. Aluminum oxide, commonly referred to as alumina, is recognized for its protective properties, particularly in environments with corrosive agents such as sodium. Alumina is an inert material, making it an effective barrier against sodium and preventing corrosion of the underlying material [23]. Additionally, the hardness of alumina makes it resistant to abrasion and wear, ensuring its longevity even in the demanding conditions found in a reactor. Equally important is alumina's excellent thermal stability, which is crucial in applications exposed to high temperatures or significant temperature changes [24]. Furthermore, silicon carbide (SiC) was also considered due to its superior heat resistance and enhanced durability in the presence of alkali catalysts. However, given our extensive and successful operational experience with the Al$_2$O$_3$ coating while using other liquid metals and the unavailability of SiC coating in a timely manner, it was decided to proceed with aluminum oxide.
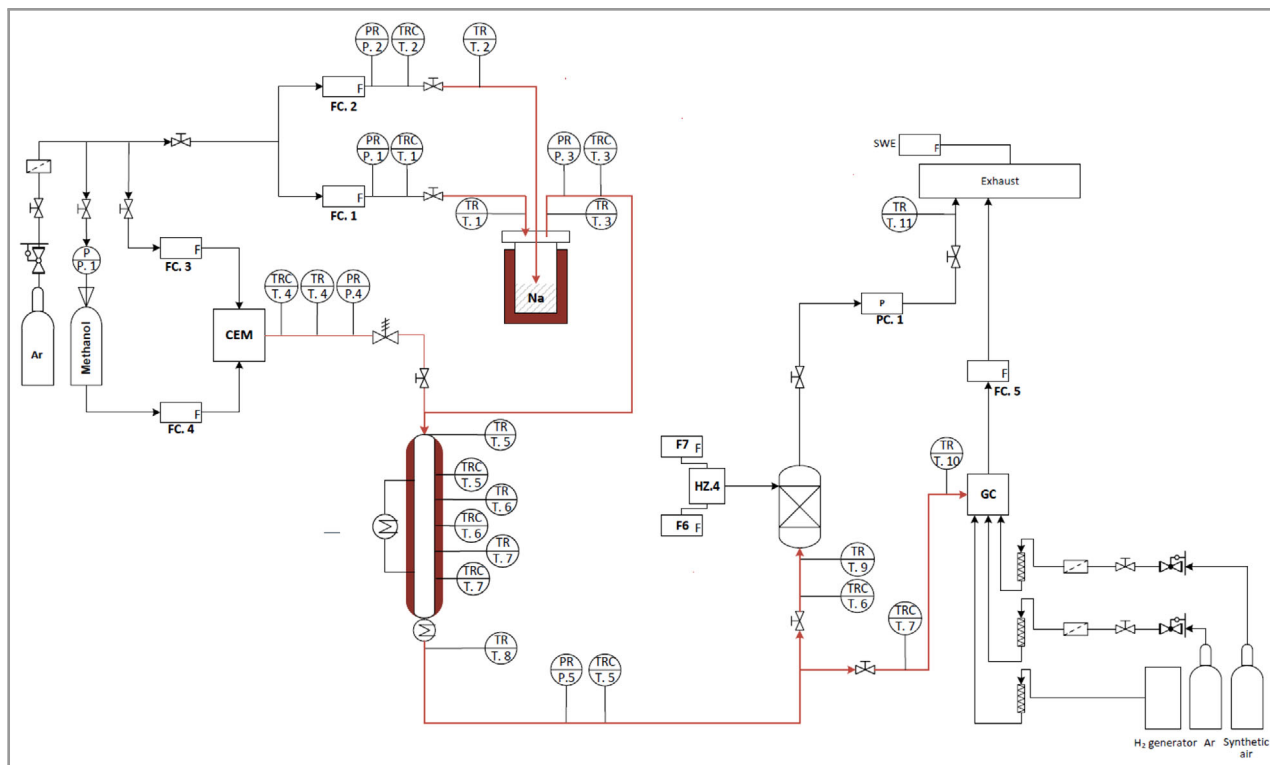
Figure 5. Process flow diagram of the MEDENA setup.

In order to evaluate the efficiency of the MEDENA (Methanol Dehydrogenation to formaldehyde using sodium (Na)) mini-plant, the conversion of methanol (Eq. (2)), the selectivity towards formaldehyde (Eq. (3)), and its yield (Eq. (4)) were determined. The above parameters were calculated as follows:

$$X_A = \frac{N_{A,0} - N_A}{N_{A,0}} \tag{2}$$

where X_A is the conversion of methanol, $N_{A,0}$ is the initial amount of methanol (mol), and N_A is the amount of methanol converted (mol).

$$S_P = \frac{N_P}{N_{A,0} - N_A} \tag{3}$$

where S_P is the selectivity towards formaldehyde, N_P is the amount of a product after reaction (mol), $N_{A,0}$ is the initial amount of methanol (mol), and N_A is the amount of methanol converted (mol).

$$Y_{P,A} = \frac{N_P}{N_{A,0}} \tag{4}$$

where $Y_{P,A}$ is the yield of a product, N_P is the amount of a product after reaction (mol), and $N_{A,0}$ is the initial amount of methanol (mol).

2.3 Methodology for the Theoretical Determination of the Amount of Evaporated Sodium

The amount of evaporated sodium is estimated by means of the Raoult-Dalton equation, which describes the phase equilibrium between the liquid sodium phase and the molar fraction of sodium in the gas phase. The equation for ideal gases and liquid phases, with $\tilde{x}_{i,Ph}$ being the mole fraction of component i in the liquid phase, p_i^* being the equilibrium vapor pressure of the pure component, $\tilde{y}_{i,Ph}$ being the partial pressure of component i in the gas phase, and p being the total vapor pressure of the solution, is shown as Eq. (5).

$$\tilde{x}_{i,Ph} \cdot p_i^* = \tilde{y}_{i,Ph} \cdot p \tag{5}$$

In the case of the bubble column, the liquid phase is composed of just one component; therefore, $\tilde{x}_{i,Ph} = 1$. Since $\tilde{y}_{i,Ph} \ll 1$, one can assume: $\tilde{y}_{i,Ph} \approx \tilde{Y}_{i,Ph}$. The Raoult-Dalton equation is therefore:

$$\widetilde{Y}_{i,Ph} = \frac{p_i^*}{p} \tag{6}$$

The vapor pressure of a substance is a function of the temperature. With increasing temperature, the vapor pressure generally grows exponentially. This is described by the Antoine equation (Eq. (7)). In the case of sodium, it can

be observed that a relatively small change in temperature can lead to a significant change in vapor pressure. The equilibrium vapor pressure is calculated by using the following Antoine equation [25]:

$$\log p = 10.182516 - \left(\frac{5693.8766}{T} \right)$$
$$- (1.0948 \log T) + 8.5874946 \times 10^{-5} T \quad (7)$$

The equation gives a value of the vapor pressure in kPa for the temperature between 300 and 2500 K. The molar flow of argon can be calculated from the volumetric flow by Eq. (8), with p_{Norm} being 101 325 Pa, $T_{Norm} = 273.15$ K, and $\tilde{R} = 8.312$ J mol^{-1}K^{-1}.

$$\dot{N}_{Ar} = \frac{p_{Norm} \cdot \dot{V}_{Ar}}{\tilde{R} \cdot T_{Norm}} \quad (8)$$

The molar balance in the bubble column is given by Eq. (9), in which $\dot{N}$ is the molar flow of sodium or argon.

$$\frac{d\dot{N}_{Na}}{dt} = 0 = \dot{N}_{Ar} \cdot \left(\tilde{Y}_{Na,in} - \tilde{Y}_{Na,out} \right) + \dot{N}_{Na} \quad (9)$$

We assume that the processes in the column have reached a steady state. Since there is no sodium in the argon stream entering the bubble column, $\tilde{Y}_{i,in} = 0$. This leads to Eq. (10).

$$\dot{N}_{Na} = \dot{N}_{Ar} \cdot \tilde{Y}_{Na,out} \quad (10)$$

If we further assume that $\tilde{Y}_{Na,out} = \tilde{Y}_{Na,Ph}$, because the loading of sodium in the gas phase at the interface is equal to the loading of sodium in the gaseous bulk phase, the mass flow of sodium ($\dot{m}_{Na}$) can be calculated with Eq. (11).

$$\dot{m}_{Na} = \dot{N}_{Na} \cdot \tilde{M}_{Na} \quad (11)$$

The description of the temperature dynamics of the argon outlet, in particular its temperature rise, is of crucial importance in the study of an argon-fed sodium bubble column. In the absence of an in situ temperature measurement inside the bubble column, there is an inevitable uncertainty concerning the accurate temperature of the sodium. In particular, since the argon outlet temperature reaches only 250 °C, it is concluded that the mass transfer likely does not occur at the expected 500 °C. This observation holds even if the heating power is adequate and the theoretical energy ratio for both sodium and argon heating is met. Hence, the considerations are as follows:

$$dh = c_p dT \rightarrow \text{for a constant } c_p \text{ value: } h - h_0 = c_p (T - T_0) \quad (12)$$

Assuming a constant isobaric heat capacity within the considered temperature range, the specific enthalpy can be evaluated by Eq. (13), which leads to Eqs. (14) and (15).

$$h(p, T) = h_0(p, T_0) + c_p \cdot (T - T_0) \quad (13)$$

$$\dot{H}(p, T) = h(p, T)\dot{m} \quad (14)$$

$$\frac{dH_{Bubble\ column}}{dt} = \dot{Q}^{in} - \dot{Q}^{out} + \dot{H}^{in} - \dot{H}^{out} \quad (15)$$

The sodium bubble column is constantly heated at 700 W; the assumed efficiency is 80 %, and therefore:

$$\dot{Q}^{in} = P_{el}\eta \quad (16)$$

The enthalpy flow that enters the bubble column can be calculated by Eq. (17).

$$\dot{H}^{in} = \dot{m}_{Ar} \cdot \left(h_{Ar,0}(p, T_0) + c_{p,Ar}\left(T_{Ar}^{in}\right) \cdot \left[T_{Ar}^{in} - T_0\right] \right)$$
$$+ \dot{m}_{Na}\left(h_{Na,0}(p, T_0) + c_{p,Na}\left(T_{Na}^{LV}\right) \right)$$
$$\cdot \left[T_{Na}^{LV} - T_0\right] + \Delta h_{Na}^{LV} \big) \quad (17)$$

The enthalpy flow that leaves the bubble column consists of argon and evaporated sodium having the same temperature (Eq. (18)).

$$\dot{H}^{out} = \dot{m}_{Ar} \cdot \left(h_{Ar,0}(p, T_0) + c_{p,Ar}\left(T_{Ar-Na}^{out}\right) \cdot \left[T_{Ar-Na}^{out} - T_0\right] \right)$$
$$+ \dot{m}_{Na}\left(h_{Na,0}(p, T_0) + \cdot c_{p,Na}\left(T_{Ar-Na}^{out}\right) \right)$$
$$\cdot \left[T_{Ar-Na}^{out} - T_0\right] \big) + \dot{m}_{Ar-Na}\Delta h_{Ar-Na}^{Mix} \quad (18)$$

Once argon and sodium mix, due to molecular interactions, the summed enthalpy flow of the individual streams differs from that of the mixed stream. However, due to the negligible amount of sodium in the stream, the enthalpy of mixing is set to zero.

The heat flow that leaves the system is equal to the heat loss of the column and the pipes (Eq. 19).

$$\dot{Q}^{out} = \sum_{losses} \dot{Q} \quad (19)$$

The calculations resulted in a highly positive change in enthalpy of the bubble column, which implies that there is no further release of heat to decrease the enthalpy, such as the cooling of sodium, occurring within the column. To further justify the temperature assumption, considering the energy requirements for argon heating, at a flow rate of 3 L min^{-1}, heating argon from an inlet temperature of 150 °C

to an assumed temperature of 500 °C requires an energy input of approximately 25 J s^{-1}. The difference between the calculated and the actual exit temperature of the argon underlines the many complexities of the system and the possible deviations from the theoretical predictions. In the process of evaluating the system dynamics, it became apparent that the argon outlet temperature consistently deviated from the originally predicted values. This observation led to an expansion of the applied model. To address this issue, mass transfer calculations were specifically performed using an adjusted benchmark temperature of 400 °C. This revised value is not only in line with the obtained data but is also supported by several sets of experimental results, making it a highly probable and representative scenario for further analysis. Considering the mass transfer of sodium into the argon bubbles, the evaporation rate is expressed by

$$\dot{N}_{Na} = A_B \beta \left(c_{Ph} - c_{B,\infty} \right) \tag{20}$$

To calculate the mass transfer coefficient, the Sherwood number (*Sh*) was used:

$$Sh = \frac{\beta \cdot d_B}{D} \tag{21}$$

The diffusion coefficient *D* was calculated from Eq. (22) derived by Aref'yev [26].

$$D = 1.05 \cdot 10^{-4} \left(\frac{T}{723} \right)^{1.65} \tag{22}$$

3 Results and Discussion

3.1 Sodium Evaporation and Condensation Experiments

Handling sodium is not only challenging in practical terms, it also requires stringent safety measures. Sodium is very reactive and carries significant risks, requiring careful precautions to prevent accidents and ensure the safety of the experimental environment. Due to the corrosive nature of sodium, several pipelines had to be exchanged during the experimental campaigns to avoid any contamination and to preserve the integrity of the facility. There were a number of operational challenges that required careful handling and maintenance during the sodium evaporation and condensation experiments. Certain components, e.g., ball valves, proved to be impractical and often clogged up within the first few minutes of testing. This slowed the progress of the trials and required constant adjustments and improvements to the apparatus. The requirement for an ultra-pure environment was essential as even the most minuscule amounts
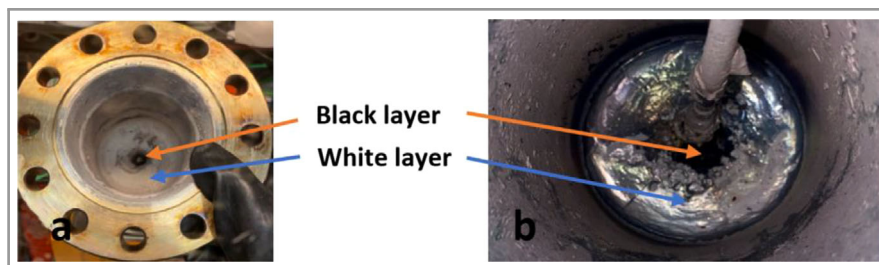
Figure 6. Sodium bubble column after the experiments.

of undesired oxygen and moisture reacted with the sodium. This interaction led to the formation of an oxide layer (its melting temperature was >1000 °C) on the surface of the sodium, which acted as a barrier preventing effective evaporation of the sodium. In addition, the reactivity of sodium with some components of the system, e.g., the sealing, resulted in corrosion of the bubble column. These findings highlighted the importance of careful control of the oxygen and water levels to ensure not only the success of the evaporation process but also the preservation of the experimental setup from corrosion. In order to identify the problematic elements, inductively coupled plasma (ICP) analyses of different sodium layers were conducted (Fig. 6). Elements such as Zn, Cu, Fe, and K were present in the bubble column after the experiments.

The use of highly pure sodium with minimal levels of calcium and potassium was indispensable. Even small traces of these impurities significantly affected the behavior of the sodium in the experimental setup. Water and oxygen may react to form calcium oxide (CaO) and calcium hydroxide (Ca(OH)$_2$). Similarly, potassium oxide (K$_2$O) and potassium hydroxide (KOH) can be formed when impurities react with potassium. Iron (Fe) and Zinc (Zn) compounds originate from stainless-steel elements and the sealing decomposition induced by sodium. The technical complexities of working with sodium highlighted the need for robust solutions to achieve reliable results. Therefore, at the end of each series of experiments, the solid residues were rinsed out to ensure an utterly uncontaminated test space.

In the high-purity sodium evaporation and condensation trials, the initial parameters were set to a flow rate of 1.9 L min^{-1}, an evaporation temperature of 450 °C, and a pressure of 1.1 bar. Under these conditions, the sodium evaporation rate was approximately 0.065 g h^{-1} (Fig. 7). In subsequent experiments, the temperature was raised to 500 °C and tests were carried out at four different flow rates: 0.8, 1.2, 1.5, and 3 L min^{-1}, all at a pressure of 1.2 bar. A clear trend was visible: As the argon flow increased, so did the amount of evaporated sodium. The results obtained at the flow rate of 0.8 L min^{-1} are of particular interest. They are relevant to the direct methanol dehydrogenation tests, as it is desirable to minimize the argon use at the industrial scale. Of the tests at this flow rate, two were run for 3 h each and a third for 6 h. The evaporation rates of sodium were
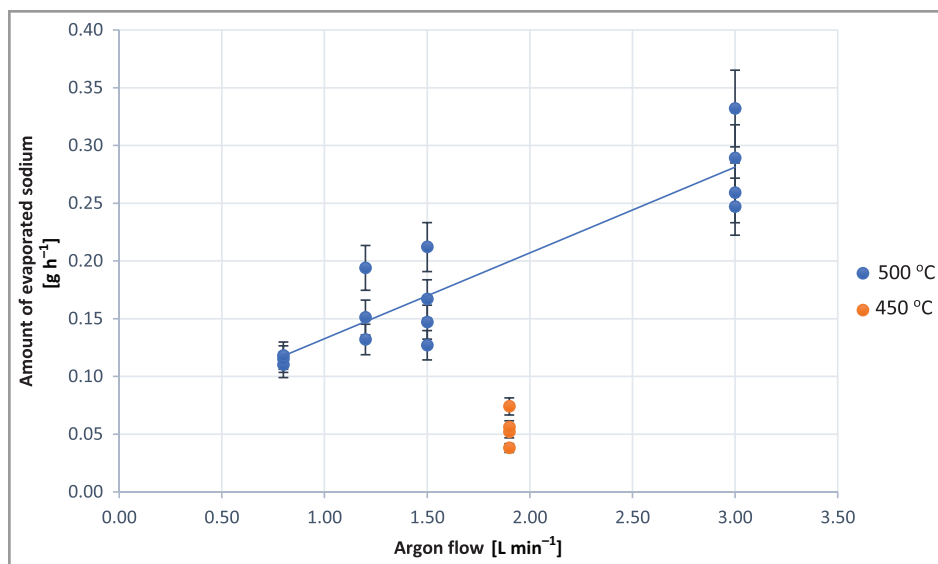
Figure 7. Experimentally determined amounts of sodium in the sodium evaporation and condensation tests (temperature of the bubble column set at 450 and 500 °C).

determined as 0.11, 0.115, and 0.118 g h^{-1}, respectively. These results indicate a consistent sodium distribution over time, confirming the reproducibility of the method.

In Fig. 8, the data from experimental trials is presented, alongside the quantity of sodium determined through mass balance evaluations. The efficiency of a bubble column is inextricably linked to its design and operating parameters. This study sets out to delineate and determine the specific parameters governing the performance of a sodium bubble column into which argon is fed. Key variables were identified and quantified through systematic experimentation and analysis, providing a basis for an improved process understanding and future scalability. In this study, the observed discrepancy between the averaged experimental results at 3 L min^{-1} and the theoretical calculations can largely be attributed to a combination of experimental inaccuracies and specific operating conditions. A unique aspect of the experiments was the possible displacement of liquid sodium from the bubble column, caused by a high argon flow. This was not considered in the mass balance approach. This is likely to have significantly contributed to the divergent

results. The findings highlight the need for further analysis in larger systems to improve the understanding and accuracy of such experimental setups.

Table 3. Parameters for the sodium bubble column.

	Argon flow [L min^{-1}]			
	0.8	1.2	1.5	3
Reynolds number of the orifice [–]	173	260	325	650
Reynolds number of the bubble [–]	26 077	30 349	33 345	46 333
Bubble diameter [mm]	11.9	13.5	14.6	18.9
Ascent velocity Mendelson [m s^{-1}]	0.30	0.31	0.31	0.34
Froude number [–]	0.78	0.72	0.69	0.61
Weber number [–]	6	7	7	11
Morton number [–]	4.69E-16			
Eötvös number [–]	7	9	11	18
Regime	constant frequency regime			
Shape	nonspherical			
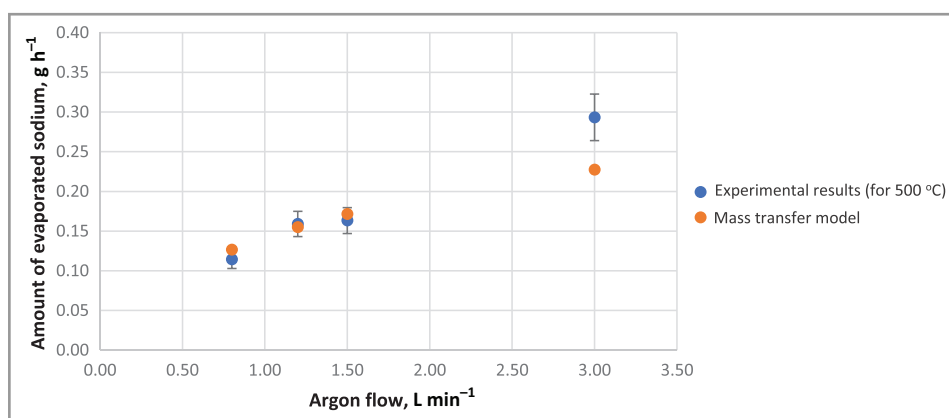
Figure 8. Comparison of the experimental values with the calculated amount of sodium using mass transfer.

Table 4. Results of the catalytic tests.

Reaction temperature [°C]	Methanol flow [g h^{-1}]	Argon flow [g h^{-1}]	Methanol mole fraction in the stream [–]	Sodium flow [g h^{-1}]	X_{CH_3OH} [%]	S_{HCHO} [%]	Y_{HCHO} [%]	Gaseous products
700	10	237	0.05	–	2	×	×	H$_2$, CO, HCOOH
550	10	237	0.05	0.114	50	45	22	H$_2$, CO, HCOOH, MeFo
700	10	237	0.05	0.032	95	72	68	H$_2$, CO, HCOOH, MeFo
800	10	237	0.05	0.012	95	63	60	H$_2$, CO, HCHO, MeFo, HCOOH
800	20	143	0.15	0.018	84	70	58	H$_2$, CO, HCHO, HCOOH
800	10	153	0.075	0.018	99	70	70	H$_2$, CO, HCHO

X, conversion; *S*, selectivity; *Y*, yield; MeFo, methyl formate.

The primary parameters for the sodium bubble column are given in Tab. 3 (Supporting Information). The presented values were calculated based on the equations listed in [27].

3.2 Catalytic Tests

Following the successfully completed sodium evaporation experiments, catalytic trials were carried out. The results of the experiments are listed in Tab. 4.

This research confirms that very low levels of sodium catalyze the reaction, as reported in [11]. Catalytic tests were conducted at various reaction temperatures, methanol concentrations, and sodium contents in the feed stream (Fig. 9).

At a temperature of 700 °C for 10 mol % methanol flow, the conversion reached 2 % without any catalyst. The observed conversion rate in the blank measurements can be attributed to the thermal decomposition of methanol. Methanol is known to undergo thermal decomposition into formaldehyde and hydrogen when exposed to high

temperatures, even in the absence of a catalyst [7, 10]. However, with the presence of the catalyst, the conversion noticeably increased to 95 %, yielding a production of 68 % of formaldehyde. At 800 °C, using sodium as a catalyst, methanol underwent nearly complete conversion, producing formaldehyde with a yield of 70 % and hydrogen as the dominant by-product, with its selectivity being >50 %. Nonetheless, it is significant to note that, as the concentration of methanol in the flow increased, the selectivity decreased (Fig. 10). Optimizing the setup to achieve higher methanol concentrations without compromising conversion and selectivity is crucial. However, increased concentrations of methanol can promote secondary or side reactions that compete with the desired formaldehyde production. At the same time, the kinetics of these side reactions may differ in relation to the methanol concentration, so that their rates may accelerate faster than the rate of the desired reaction, leading to reduced selectivity. Addionally, sodium was found in metallic form at the gas scrubber inlet, meaning that it can be partially or fully recovered.
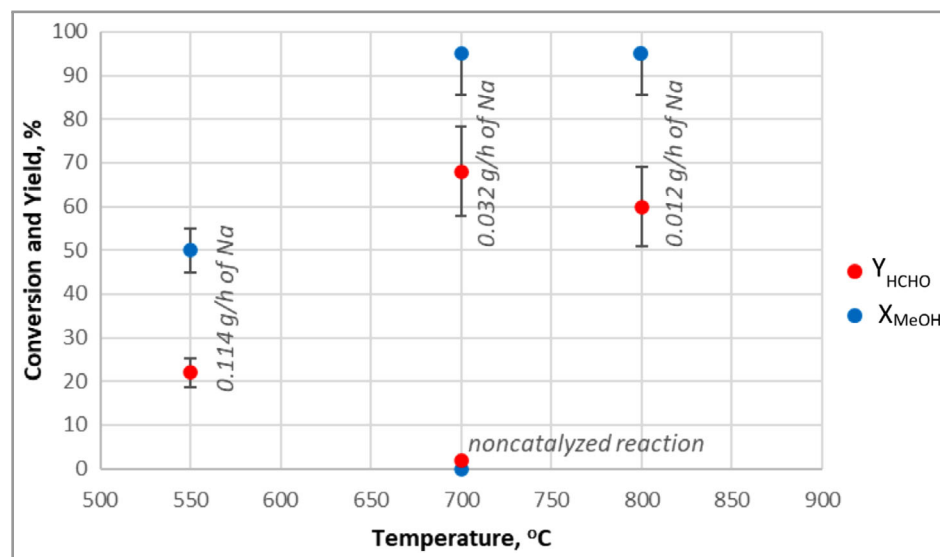
Figure 9. Experimental results showing the temperature dependence on conversion and yield for the molar MeOH concentration of 0.05.
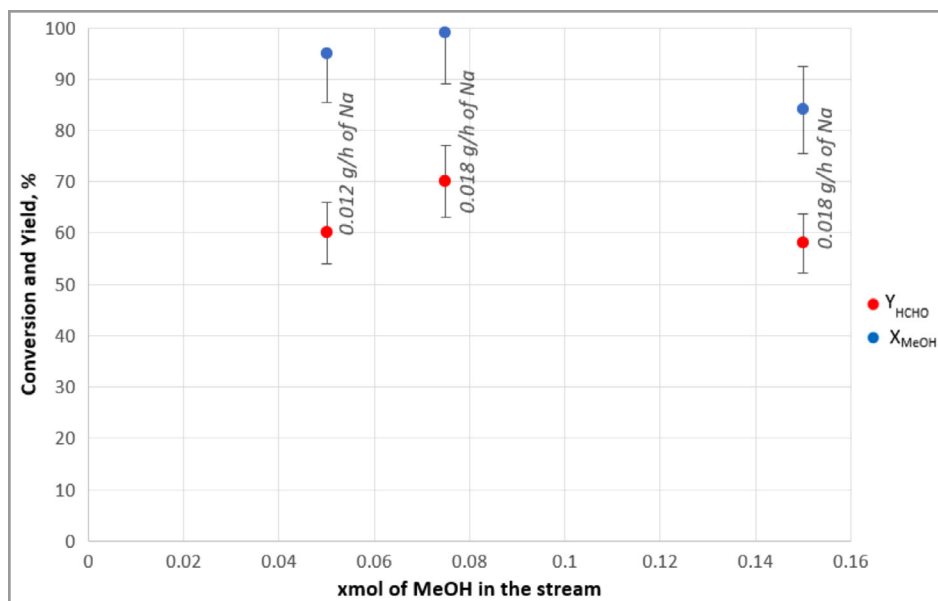
Figure 10. Experimental results showing the influence of the molar concentration of methanol on the conversion and yield.

4   Conclusions

An experimental setup to investigate catalytic dehydrogenation of methanol to formaldehyde has been developed, with sodium vapor as catalyst. The setup includes a newly developed sodium vapor dosing system as one of the main components, which generates a mixture of sodium vapor and inert carrier gas. By varying the flow rates of the inert gas and the temperature of the sodium bubble column, it was demonstrated that accurate and constant catalyst dosing could be achieved over an extended period of time (for several weeks, the sodium in the bubble column did not need to be replaced). To conclude, in this study an almost complete methanol conversion at 800 °C was achieved, with a formaldehyde yield of 70 % and with hydrogen as the major by-product. In addition, the experimental results are consistent with established literature data and confirm observations from similar experiments in which sodium metal was used as catalyst. Namely, as the methanol content in the stream increased, the yield of formaldehyde decreased. However, the use of sodium as catalyst resulted in high yields of both hydrogen and formaldehyde.

Author Contributions

M. Kamienowska: design, calculations, experimental tests, formal analysis and visualization, original draft, review & editing. M. P. Deutschmann: experimental tests, analysis, calculations, reviewing & editing. M. Bender: funding acquisition, supervision, reviewing & editing. L. Stoppel: technical design, funding acquisition. M. Daubner: design of sodium evaporation and condensation elements. T. Wetzel: funding acquisition, supervision, reviewing & editing.

K. Niedermeier: conceptualization, supervision, reviewing & editing.

Supporting Information

Supporting information for this article can be found under DOI: https://doi.org/10.1002/cite.202400007.

Symbols used

c	[mol m^{-3}]	molar concentration
d	[m]	diameter
D	[m^{2}s^{-1}]	diffusion coefficient
$\dot{H}$	[J s^{-1}]	enthalpy flow rate
$\dot{m}$	[g h^{-1}]	mass flow
N	[mol]	amount of a substance
$\dot{N}$	[mol h^{-1}]	mole flow
$\dot{Q}$	[W]	heat flow rate
p	[Pa, bar]	pressure
P	[W]	power
R	[J mol^{-1}K^{-1}]	universal gas constatnt

Re	[–]	Reynolds number
S	[%]	selectivity towards a product
Sh	[–]	Sherwood number
t	[h]	time
T	[°C, K]	temperature
x	[–]	mole fraction of the component in the liquid phase
X	[%]	conversion of a substrate
y	[–]	mole fraction of the component in the gas phase
Y	[%]	yield of a product
$\dot{V}$	[m³h⁻¹]	volumetric flow rate (normal conditions)

Greek symbols

β	[m s⁻¹]	mass transfer coefficient
ρ	[g L⁻¹]	density
σ	[N m⁻¹]	surface tension

Sub-/superscripts

0	initial conditions
A	substrate
B	bubble
Cat	catalyst
el	electrical power
i	component index
In	inlet
Mix	mixture
N	standard conditions (273.15 K, 1 atm)
O	orifice
Out	outlet
P	product
PA	all products and unreacted components
Ph	phase

References

[1] F. Eichner, E. Turan, J. Sauer, M. Bender, S. Behrens, *Catal. Sci. Technol.* **2023**, *13* (*8*), 2349–2359. DOI: https://doi.org/10.1039/D2CY01405J

[2] H. I. Mahdi, N. N. Ramlee, D. H. da Silva Santos, D. A. Giannakoudakis, L. H. de Oliveira, R. Selvasembian, N. I. W. Azelee, A. Bazargan, L. Meili, *Mol. Catal.* **2023**, *537*, 112944. DOI: https://doi.org/10.1016/j.mcat.2023.112944

[3] M. Qian, M. A. Liauw, G. Emig, *Appl. Catal., A* **2003**, *238* (*2*), 211–222. DOI: https://doi.org/10.1016/S0926-860X(02)00340-X

[4] A. M. Bahmanpour, A. Hoadley, A. Tanksale, *Rev. Chem. Eng.* **2014**, *30* (*6*), 583–604. DOI: https://doi.org/10.1515/revce-2014-0022

[5] J. Thrane, U. V. Mentzel, M. Thorhauge, M. Høj, A. D. Jensen, *Catalysts* **2021**, *11* (*11*), 1329. DOI: https://doi.org/10.3390/catal11111329

[6] N. Y. Usachev, I. Krukovsky, S. A. Kanaev, *Pet. Chem.* **2004**, *44*, 379–394.

[7] J. Sauer, G. Emig, *Chem. Eng. Technol.* **1995**, *18* (*4*), 284–291. DOI: https://doi.org/10.1002/ceat.270180410

[8] S. Ruf, G. Emig, *Appl. Catal., A* **1997**, *161* (*1*), L19–L24. DOI: https://doi.org/10.1016/S0926-860X(97)00127-0

[9] R. Maurer, A. Renken, *Chem. Eng. Res. Des.* **2003**, *81* (*7*), 730–734. DOI: https://doi.org/10.1205/026387603322302896

[10] S. Ruf, Die Natrium-katalysierte Dehydrierung von Methanol zu wasserfreiem Formaldehyd, *Dissertation*, Technische Fakultät der Universität Erlangen-Nürnberg, Erlangen **1998**.

[11] S. Ruf, A. May, G. Emig, *Appl. Catal., A* **2001**, *213*, 203–215. DOI: https://doi.org/10.1016/S0926-860X(00)00904-2

[12] Y. Dai, X. Zheng, P. Ding, *Nucl. Eng. Technol.* **2021**, *53* (*11*), 3474–3490. DOI: https://doi.org/10.1016/j.net.2021.05.021

[13] P. C. S. Wu, B. R. Grundy, R. L. Miller, *Metall. Trans. A* **1979**, *10* (*3*), 319–325. DOI: https://doi.org/10.1007/BF02658340

[14] A. W. Thorley, C. Tyzack, *Liq. Alkali Met., Proc. Int. Conf. BNES Nottingham* **2013**, pp. 257–273.

[15] D. T. Hoelzer, C. P. Massey, S. J. Zinkle, D. C. Crawford, K. A. Terrani, *J. Nucl. Mater.* **2020**, *529*, 151928. DOI: https://doi.org/10.1016/j.jnucmat.2019.151928

[16] T.-L. Sham, L. Tan, Y. Yamamoto, in *Int. Conf. Fast React. Related Fuel Cycles Safe Technol. Sust. Scenarios (FR13)*, Paris **2013**.

[17] H. Kim, J. G. Gigax, J. Fan, F. A. Garner, T.-L. Sham, L. Shao, *J. Nucl. Mater.* **2019**, *527*, 151818. DOI: https://doi.org/10.1016/j.jnucmat.2019.151818

[18] S. Handschuh-Wang, T. Wang, L. Zhu, Y. Xu, L. Huang, T. Gan, Y. Tang, X. Zhou, *ACS Appl. Mater. Interfaces* **2020**, *12* (*36*), 40891–40900. DOI: https://doi.org/10.1021/acsami.0c09428

[19] S. Malang, H. U. Borgstedt, E. H. Farnum, K. Natesan, I. V. Vitkovski, *Fusion Eng. Des.* **1995**, *27*, 570–586. DOI: https://doi.org/10.1016/0920-3796(95)90172-8

[20] M. A. Markov, A. D. Kashtanov, A. V. Krasikov, A. D. Bykova, D. A. Gerashchenkov, A. M. Makarov, S. N. Perevislov, *Key Eng. Mater.* **2019**, *822*, 752–759. DOI: https://doi.org/10.4028/www.scientific.net/KEM.822.752

[21] J.-B. Vogt, I. Proriol Serre, *Coatings* **2021**, *11* (*1*), 53. DOI: https://doi.org/10.3390/coatings11010053

[22] F. A. Kozlov, V. V. Alexeev, Y. P. Kovalev, V. Y. Kumaev, V. V. Matyuchin, E. A. Orlova, E. P. Pirogov, A. P. Sorokin, S. I. Shcherbakov, *At. Energy* **2012**, *112* (*1*), 21–28. DOI: https://doi.org/10.1007/s10512-012-9519-4

[23] T. Dursun, C. Soutis, *Mater. Des. (1980–2015)* **2014**, *56*, 862–871. DOI: https://doi.org/10.1016/j.matdes.2013.12.002

[24] F. Czerwinski, *Materials (Basel)* **2020**, *13* (*15*), 3441. DOI: https://doi.org/10.3390/ma13153441

[25] https://publica.fraunhofer.de/handle/publica/159135 (accessed on September 13, 2023).

[26] T. Kumada, R. Ishiguro, Y. Kimachi, *Nucl. Sci. Eng.* **1979**, *70* (*1*), 73–81. DOI: https://doi.org/10.13182/NSE79-A18929

[27] T. G. Geißler, Methanpyrolyse in einem Flüssigmetall-Blasensäulenreaktor, *Dissertation*, Karlsruher Institut für Technologie, Karlsruhe **2017**. https://publikationen.bibliothek.kit.edu/1000076151 (accessed Sept. 17, 2023).